Environment International 185 (2024) 108532

Contents lists available at ScienceDirect

Environment International

journal homepage: www.elsevier.com/locate/envint

Full length article

The size-dependence and reversibility of polystyrene nanoplastics-induced lipid accumulation in mice: Possible roles of lysosomes

Yan-Yang Lu [a], Lu Lu [b], Hong-Yun Ren [a], Weizhen Hua [c], Nengxing Zheng [c], Fu-Yi Huang [a], Jiani Wang [a], Meiping Tian [a], Qingyu Huang [a,*]

[a] Key Lab of Urban Environment and Health, Institute of Urban Environment, Chinese Academy of Sciences, 1799 Jimei Road, Xiamen 361021, China
[b] College of Resources and Environment, Fujian Agriculture and Forestry University, Fuzhou 350002, China
[c] Department of Health Inspection and Quarantine, School of Public Health, Fujian Medical University, Fuzhou 350122, China

ARTICLE INFO

Keywords:
Nanoplastics
Hepatic lipid accumulation
Autophagy
Lysosome
Reversibility

ABSTRACT

Nanoplastics (NPs) continue to accumulate in global aquatic and terrestrial systems, posing a potential threat to human health through the food chain and/or other pathways. Both *in vivo* and *in vitro* studies have confirmed that the liver is one of the main organs targeted for the accumulation of NPs in living organisms. However, whether exposure to NPs induces size-dependent disorders of liver lipid metabolism remains controversial, and the reversibility of NPs-induced hepatotoxicity is largely unknown. In this study, the effects of long-term exposure to environmentally relevant doses of polystyrene nanoplastics (PS-NPs) on lipid accumulation were investigated in terms of autophagy and lysosomal mechanisms. The findings indicated that hepatic lipid accumulation was more pronounced in mice exposed to 100 nm PS-NPs compared to 500 nm PS-NPs. This effect was effectively alleviated after 50 days of self-recovery for 100 nm and 500 nm PS-NPs exposure. Mechanistically, although PS-NPs exposure activated autophagosome formation through ERK (mitogen-activated protein kinase 1)/mTOR (mechanistic target of rapamycin kinase) signaling pathway, the inhibition of Rab7 (RAB7, member RAS oncogene family), CTSB (cathepsin B), and CTSD (cathepsin D) expression impaired lysosomal function, thereby blocking autophagic flux and contributing to hepatic lipid accumulation. After termination of PS-NPs exposure, lysosomal exocytosis was responsible for the clearance of PS-NPs accumulated in lysosomes. Furthermore, impaired lysosomal function and autophagic flux inhibition were effectively alleviated. This might be the main reason for the alleviation of PS-NPs-induced lipid accumulation after recovery. Collectively, we demonstrate for the first time that lysosomes play a dual role in the persistence and reversibility of hepatotoxicity induced by environmental relevant doses of NPs, which provide novel evidence for the prevention and intervention of liver injury associated with nanoplastics exposure.

1. Introduction

The advent of plastics is a history of innovation, providing significant convenience to worldwide manufacturing and everyday existence. However, the surge in plastic pollution has become an escalating environmental crisis in the current era. As of 2020, global plastic production had surged to nearly 10 billion tons, with roughly 80% of the resulting plastic waste persisting in the natural environment (Geyer et al., 2017; UNEP, 2021). Over time, plastic waste undergoes photodegradation, mechanical abrasion, biodegradation, and/or other processes to progressively break down into small-sized plastic debris, namely nano/microplastics (NMPs). Those with particle sizes smaller than 5 mm are classified as microplastics (MPs). While there is still debate over whether the upper size limit for nanoplastics is 100 nm or 1000 nm, the scientific community generally accepts that plastic debris ranging from 1 to 1000 nm are considered nanoplastics (NPs) (Gigault et al., 2018; Gonçalves and Bebianno, 2021; WHO, 2022). Increasing numbers of studies have demonstrated the presence of NMPs in air (Klein and Fischer, 2019), drinking-water (Samandra et al., 2022), and food (Van Cauwenberghe and Janssen, 2014), indicating possible health risks to humans associated with exposure to NMPs through inhalation, ingestion and/or dermal contact. Recently, NMPs have been detected in the blood of healthy individuals, with concentrations as high as 1.6 μg/mL (Leslie et al., 2022). Once the environmental pollutants enter the human

* Corresponding author.
E-mail address: qyhuang@iue.ac.cn (Q. Huang).

https://doi.org/10.1016/j.envint.2024.108532
Received 3 January 2024; Received in revised form 2 February 2024; Accepted 22 February 2024
Available online 24 February 2024

bloodstream, they can be easily transferred to peripheral organs. Notably, Horvatits et al. (2022) have discovered 4.6 to 11.9 particles/g in liver tissue samples of patients with cirrhosis. Furthermore, this study pointed out that even in control populations without hepatic disease, a certain amount of NMPs was also observed, with concentrations ranging from 0.3 to 1.9 particles/g. Therefore, further investigation into NMPs-induced hepatotoxicity is imperative.

The liver is widely recognized as a pivotal organ in lipid metabolism. The influence of NMPs exposure on lipid metabolism has gained much attention in recent years. For example, exposure of 1 μm polystyrene (PS) NMPs resulted in elevated levels of total triglyceride (TG) and excessive deposition of lipid droplets in liver organoids (Cheng et al., 2022). Similarly, in high-fat diet fed mice, chronic oral exposure to 60 nm-sized PS NMPs exacerbated hepatic lipid accumulation, possibly due to enhanced intestinal barrier permeability and metabolic stress (Shiu et al., 2022). In contrast, the levels of serum and hepatic TG were reduced in mice following exposure to 2 μm polyvinyl chloride (PVC) NMPs for 60 days (Chen et al., 2022). Lu et al. (2018) also found that mice exposed to 1000 μg/L of 0.5 and 50 μm PS NMPs for 5 weeks decreased TG synthesis and disturbed hepatic lipid metabolism rather than inducing lipid accumulation. Obviously, there remains controversy regarding the effect of NMPs with different particle sizes on lipid metabolism, which requires further validation.

It is worth noting that NMPs belong to a class of chemically stable solid particles that are difficult to degrade or decompose in living organisms. These NMPs accumulated in cells could be removed through the exocytosis pathway (Sakhtianchi et al., 2013; Liu et al., 2021), thereby raising concerns regarding the persistence or reversibility of NMPs toxicity. Han et al. (2023) suggested that the changes in gut microbiota diversity induced by acute NMPs exposure in *Eriocheir sinensis* could return to near-normal levels after a certain period of recovery, whereas hepatopancreas damage remained irreversible during the recovery period. Similarly, the survival rate of juvenile large yellow croaker *Larimichthys crocea* following NMPs treatment was significantly lower than that in the control group during both the exposure and recovery periods, and the activities of superoxide dismutase (SOD) and catalase (CAT), two markers of oxidative stress, remained elevated above the baseline in the liver after recovery under high concentration NMPs treatment, showing poor self-recovery effects (Li et al., 2021a). However, oxidative stress induced by NMPs in diatoms (*Phaeodactylum tricornutum*) at environmentally relevant concentrations was reversible (Yao et al., 2023). Obviously, the research on the persistence or reversibility of NMPs toxicity mainly focused on a few aquatic organisms. Whether NMPs accumulated in the liver of terrestrial organisms could be excreted from the body and thus alleviate lipid metabolism disorders after termination of NMPs exposure remain to be elucidated.

Autophagy, also known as macroautophagy, is a highly conserved cellular process in eukaryotes that involves the degradation of cytoplasmic waste in lysosomes. This multistep pathway includes autophagic cargo recognition, autophagosome formation, autophagosome-lysosome fusion, as well as the subsequent degradation and recycling of autophagic cargo (Yamamoto et al., 2023). The quantification of autophagic degradation activity is commonly known as autophagic flux (Klionsky et al., 2012). Under physiological conditions, maintaining basal levels of autophagic flux is crucial for metabolic homeostasis in liver (Ueno and Komatsu, 2017). However, impaired autophagy can inhibit decomposition of lipid droplets, thereby inducing excessive lipid accumulation and inflammation, and even exacerbating liver fibrosis and cancer (Ueno and Komatsu, 2017; Scorletti and Carr, 2022). Furthermore, recent research has highlighted that abnormal autophagy triggered by environmental pollutants is increasingly recognized as a noteworthy factor in the disruption of lipid metabolism and hepatic impairment. For instance, the food contaminant 1,3-dichloro-2-propanol (1,3-DCP) was found to induce hepatic lipid accumulation by inhibiting autophagy through thymoma viral proto-oncogene 1(AKT)/mechanistic target of rapamycin kinase (mTOR)/forkhead box O1(FOXO1) signaling pathway in mice (Fan et al., 2021). Lysosomes, the acidic organelles with numerous hydrolytic enzymes, participate in autophagic degradation through fusion with autophagosomes. The efficient progression of autophagic flux is largely dependent on lysosomal activity and function. Zhao et al. (2022) confirmed that lead (Pb) impaired lysosome formation and activity mediated by transcription factor EB (TFEB), thereby blocking the autophagic flux and ultimately aggravating the lipid accumulation in human hepatocellular carcinoma (HepG2) cells. Similarly, exposure to bisphenol A (BPA) decreased the translocation of Syntaxin 17 (Stx17) to lysosomes, leading to a defect in autophagosome-lysosome fusion, which was responsible for abnormal accumulation of lipid droplets (Yang et al., 2017; Song et al., 2019). For NMPs, the co-exposure to arsenic and 500 nm PS NMPs induced autophagy and inhibited autophagic degradation in mouse liver (Zhong et al., 2022). However, whether NMPs-induced lipid accumulation was associated with autophagy-lysosome pathway has not been established.

It is worth noting that with advancements in detection technology, NPs have been detected in rivers, seas, and nature reserves across Asia, Europe, Antarctica, and the Arctic Ocean (Shi et al., 2023). Recent research has also revealed the widespread occurrence of NPs with particle sizes ranging from 100 nm to 500 nm in bottled drinking water; furthermore, there is a higher abundance of NPs at approximately 100 nm and 500 nm sizes (Huang et al., 2022; Zhang et al., 2023). Additionally, PS emerged as one of the predominant types detected in human liver samples (Horvatits et al., 2022). Therefore, considering these factors collectively, polystyrene nanoplastics with particle sizes of 100 nm and 500 nm (referred to as "100 nm PS-NPs" and "500 nm PS-NPs") were chosen for the investigation of their hepatotoxicity at an environmentally relevant concentration in this study. The objectives are three-fold: (1) to confirm whether exposure to PS-NPs could induce lipid accumulation with particle size dependence; (2) to elucidate the effects of exposure to PS-NPs on the autophagy-lysosome pathway; (3) to clarify whether PS-NPs-induced liver damage could be reversed after a period of recovery. This study offers novel insights into the potential impact of NPs on lipid metabolism, which is critical for assessing the health risks of NPs.

2. Materials and methods

2.1. Nanoplastics characteristics

Two types of commercial PS-NPs suspensions were used in this study. One type was spherical PS-NPs with diameters of 100 nm and 500 nm (2.5% w/v in ultrapure water), which was obtained from the BaseLine ChromTech Research Centre (Tianjin, China). The other type of 100 nm and 500 nm PS-NPs was filled with green fluorescent substances, exhibiting excitation and emission wavelengths at 470 and 525 nm, respectively (Hugebio Biotechnology Company, Shanghai, China). It is important to note that there are no fluorescent materials attached to the surface of these particles. The morphological characteristics, size distribution, and chemical composition of the particles were verified using a scanning electron microscope (SEM, S-4800, Hitachi, Japan), a particle size analyzer (Malvern Zetasizer Nano-ZS, Model ZEN3600, UK) and a LabRAM Aramis confocal Raman microscope (Horiba Jobin Yvon, USA), respectively. In addition, the fluorescence stability was determined by measuring the fluorescence intensity of 100 nm and 500 nm fluorescent PS-NPs using a microplate reader (Spark, Tecan, Switzerland) after two months of incubation in a dark environment at 37 °C.

2.2. Animals and PS-NPs treatment

All male C57BL/6 mice (six-weeks old) were purchased from the SLAC Laboratory Animal Center (Shanghai, China), and maintained in cages with free access to animal chow and water under a specific pathogen-free condition (22 ± 2 °C room temperature, 55 ± 5% relative humidity and a 12/12 h light/dark cycle). All animal experiments were

performed in accordance with the relevant guidelines of the Institutional Animal Ethics Committee of the Institute of Urban Environment, Chinese Academy of Sciences. For the long-term toxicity experiment, the mice in the exposed groups were administered a diet containing 100 nm and 500 nm PS-NPs at a concentration of 0.1 g/kg for a duration of 180 days, respectively. This dosage was determined based on the dose of environmental exposure for humans. On a global scale, the estimated per capita intake of NMPs through various exposure routes ranges from 0.1 to 5 g/week (approximately equivalent to 14–700 mg/day) (Senathirajah et al., 2021), which corresponds to 0.2–10 mg/kg body weight (bw), assuming an average bw of 70 kg/person. Thereafter, using a classical pharmacological and toxicological formulation (Nair and Jacob, 2016), the equivalent dose in mice is calculated to be 2.46–123 mg/kg bw based on the human daily intake dose. Considering a daily food intake of 2–5 g per mouse and a bw range of 20–35 g, our dose (0.1 g/kg food) corresponds to an exposure dose of 10–14.4 mg/kg bw in mice, which falls well within the estimated mice equivalent dose. Mice in the 180-day control group received a standard rodent chow diet. The corresponding recovered groups for 100 nm and 500 nm PS-NPs exposed groups were that the mice continued to be fed a standard rodent chow diet for 50 days after the exposure, and the 230-day control group was also set up ($n = 5$).

For the biodistribution experiment, the mice in two exposed groups were treated with 100 nm and 500 nm fluorescent PS-NPs at the concentration of 0.2 mg/mL, respectively. The fluorescent PS-NPs was diluted in drinking water, and the mice were continuously exposed for 30 days. With a daily water intake of approximately 5 mL, this dose corresponds to an intake of 1 mg per mouse per day, which is slightly higher than the dose used for the long-term toxicity exposure described above, for the purpose of enhancing the detectability of fluorescent PS-NPs. The mice in the control group drank fluorescent PS-NPs-free water. The two restored groups were mice subjected to an additional 30-day period of normal water consumption after being exposed to 100 nm and 500 nm fluorescent PS-NPs, respectively. The recovered control group was also set up where mice consumed normal water for 60 days.

To avoid the possible MPs/NPs contamination in the laboratory environment, glassware or metal consumables were used for mouse drinking water and food containers, dissection-related supplies, and storage tubes for samples.

2.3. Cell culture

The human hepatocellular carcinoma cell line (HepG2) suitable for studying lipid metabolism was purchased from Cell Bank of Type Culture Collection, Chinese Academy of Sciences (Shanghai, China). Cells were cultured in MEM (Gibco, NY, USA) supplemented with 1.5 g/L $NaHCO_3$, 0.11 g/L sodium pyruvate, and 10% fetal bovine serum (HyClone, Victoria, Australia) in a humidified incubator containing 5% CO_2 at 37 ℃.

2.4. Fluorescent PS-NPs biodistribution

At the end of the fluorescent PS-NPs exposure, the mice were sacrificed, and their liver tissues were collected. Subsequently, these fresh liver samples were immediately imaged using an IVIS Lumina II imaging system (PerkinElmer, USA) equipped with a charge coupled device (CCD) camera. The 465 nm excitation filter and the GFP emission filter were selected to detect the fluorescent signals of the mouse liver. The exposure time was set to 60 s. The acquisition and analysis of the data were performed using the Living Image 4.3.1 software.

2.5. Lipid index assays

TG and total cholesterol (TC) in liver tissues were measured by commercial kits (Nanjing Jiancheng, jiangsu, China) according to the manufacturer's protocols. The absorbance was measured at 510 nm using a microplate reader (Spark, Tecan, Switzerland).

2.6. Oil-Red-O assay

Lipid accumulation was visualized by Oil-Red-O staining. Briefly, frozen hepatic sections were fixed and stained with Oil-Red-O worksolution for 10 min, then differentiated with 60% isopropanol, counterstained with hematoxylin and mounted in glycerin jelly. The images were captured using an Olympus CKX41 light microscope (Tokyo, Japan).

2.7. mRNA expression

Total RNA was extracted from mouse liver samples using the TRIzol reagent (Thermo Fisher Scientific, MA, USA) and reversely transcribed with HiScript III RT SuperMix for qPCR (+gDNA wiper) (Vazyme, Nanjing, China). Real-time PCR was performed using the ChamQ SYBR qPCR Master Mix (Vazyme) on a LightCycler®480 Instrument II (Roche, Basle, Switzerland).

2.8. Western blot analysis

Total protein of mouse liver was prepared using RIPA buffer (Thermo Fisher Scientific), and the concentrations were measured using the BCA protein assay kit (Thermo Fisher Scientific). Equal amounts of protein were subjected to gel electrophoresis and blotted on PVDF membranes. Then, the membranes were blocked and incubated with antibodies against sterol regulatory element binding transcription factor 1/Srebf1 (Abcam, #ab28481, 1:2000), fatty acid binding protein 1/Fabp1 (Cell Signaling Technology, #13368, 1:1000), acyl-Coenzyme A oxidase 1, palmitoyl/Acox1 (Abcam, #ab184032, 1:2000), carnitine palmitoyltransferase 1a/Cpt1a (Abcam, #ab234111, 1:2000), apolipoprotein C-III/Apoc3 (Abcam, #ab108205, 1:2000), microtubule-associated protein 1 light chain 3 beta/LC3B (Abcam, #ab192890, 1:2000), sequestosome 1/p62 (Abcam, #ab109012, 1:10000), autophagy related 5/ATG5 (Abcam, #ab108327, 1:2000), Beclin 1 (Abcam, #ab207612, 1:2000), mitogen-activated protein kinase 1/ERK (Abcam, #184699, 1:10000), Phospho-ERK (Abcam, #ab201105, 1:1500), mTOR (Abcam, #ab134903, 1:10000), Phospho-mTOR (Ser2448) (Abcam, #ab109628, 1:2000), RAB7, member RAS oncogene family/Rab7 (Abcam, #ab137209, 1:5000), cathepsin B/CTSB (Cell Signaling Technology, #31718, 1:1000), cathepsin D/CTSD (Abcam, #ab75852, 1:2000), and β-actin (Cell Signaling Technology, #4970, 1:2000). The antibody-reactive bands were visualized by ECL chemiluminescence detection system (WesternBright™ ECL HRP substrate, Advansta, CA, USA), and quantified by Image-Pro Plus 6.0 software (Media Cybernetics, MD, USA).

2.9. Transmission electron microscope (TEM) observation

TEM-based observation was performed to determine PS-NPs-induced autophagosomes in mouse liver at the ultrastructural levels. A small portion of mouse liver samples in the exposed and control groups were cut into small pieces, and fixed in 2.5% glutaraldehyde for 2 h at 4 °C, followed by post-fixed with 1% osmium acid for 1 h. Then, the samples were dehydrated in a graded ethanol series and acetone, and embedded in Spurr resin. The ultrathin sections were acquired using an ultramicrotome (Leica UC7, Germany), and subsequently stained with uranyl acetate. Finally, the autophagosomes of the liver samples were visualized under a TEM (H-7650, Hitachi, Japan).

2.10. Localization of fluorescent PS-NPs in lysosomes in vitro

HepG2 cells were exposed to 20 μg/mL of 100 nm and 500 nm green fluorescent PS-NPs, respectively. After a 24-h exposure, cells were incubated for 30 min with 50 nM LysoTracker Red DND-99 (Invitrogen,

USA), a dye that labeled lysosomes with red fluorescence. The stained HepG2 cells were immediately photographed with a LSM 710 Laser Scanning Confocal Microscope (Zeiss, Jena, Germany). The signal overlap between green and red channels, as shown by the yellow pixels, represented the entry of the exposed PS-NPs into lysosomes in HepG2 cells.

2.11. Lysosomal exocytosis

An activator (ionomycin) and an inhibitor (bafilomycin A1) were used to explore the exocytosis pathway *in vitro*. Ionomycin is an ionophore that increases intracellular calcium to promote the fusion of the lysosome to cell membrane (Ding et al., 2018), while bafilomycin A1 is a late-phase autophagy inhibitor used for the suppression of lysosomal acidification (Yanes et al., 2013). Briefly, HepG2 cells were exposed to 20 μg/mL of 100 nm and 500 nm fluorescent PS-NPs for 24 h, respectively. Subsequently, the exposed cells were incubated with 100 nM bafilomycin A1 or 10 μM ionomycin (MedChemExpress, New Jersey, America) for 3 h. The experimental groups were set as follows: the 100 nm PS-NPs group, the 100 nm PS-NPs + ionomycin group, and the 100 nm PS-NPs + bafilomycin A1 group; the 500 nm PS-NPs group, the 500 nm PS-NPs + ionomycin group, and the 500 nm PS-NPs + bafilomycin A1 group. Intracellular fluorescence intensity was quantified using a microplate reader (Spark, Tecan, Switzerland) following a 9-h incubation in fresh medium, and normalized to the number of cells.

2.12. Statistical analysis

The data analysis was performed using an SPSS software (Version 19.0). Two-group comparison was analyzed using unpaired Student's *t* test. Statistical differences were considered as significant at $p < 0.05$.

3. Results

3.1. PS-NPs characteristics

The SEM images showed that the morphology of the studied PS-NPs was all spherical with uniform size (Fig. 1**A**). The particle size distribution was depicted in Fig. 1**B**, and the average diameters of 100 nm and 500 nm PS-NPs, as well as 100 nm and 500 nm fluorescent PS-NPs, dispersed in ultrapure water were approximately 103.1, 514.9, 107.2, and 539.2 nm, respectively. For fluorescent PS-NPs, since the normal temperature of the experimental mice was 37 ± 1 ℃, we investigated the fluorescence attenuation at 37 ℃, and found that the fluorescence intensity of 100 nm and 500 nm fluorescent PS-NPs did not significantly decrease after two months of incubation in the dark at 37 ℃ (Fig. 1**C**), indicating that both sizes of fluorescent PS-NPs could effectively maintain their fluorescence stability, thereby fulfilling the requirements for the following biodistribution analysis. For PS-NPs without fluorescent labeling, Raman spectrometry confirmed that the chemical composition of these particles used for the long-term toxicity experiment was polystyrene (PS) (Fig. 1**D**). This result was consistent with the Raman spectrometry of the PS standard substance (Wright et al., 2019).

3.2. PS-NPs biodistribution

The biodistribution of 100 nm and 500 nm fluorescent PS-NPs in the mouse liver was monitored by an *ex vivo* fluorescence imaging system.

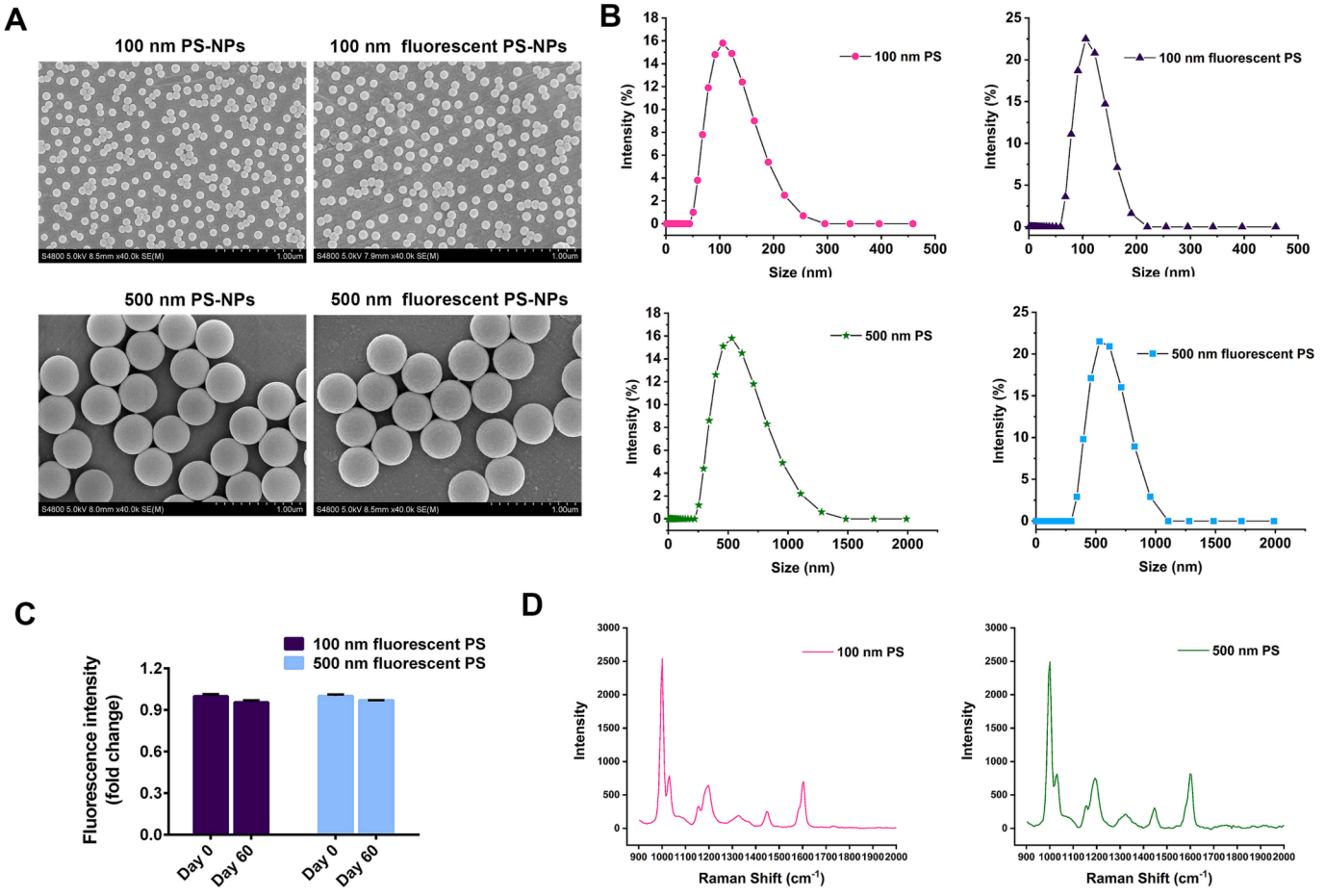

Fig. 1. Characterization of PS-NPs with different particle sizes. (A) SEM micrographs. (B) Size distribution. (C) Changes in fluorescence intensity of 100 nm and 500 nm fluorescent PS-NPs after two months of incubation at 37 ℃ in the dark. (D) Raman spectra of 100 nm and 500 nm PS-NPs.

As depicted in Fig. 2**A and B**, the fluorescence intensities of the liver were significantly increased in the 100 nm and 500 nm PS-NPs-exposed groups compared to the 30-day control group. Following a recovery period of 30 days, there was a significant decrease in liver fluorescence intensity in the 100 nm and 500 nm PS-NPs-restored groups. These results indicated that both the 100 nm and 500 nm PS-NPs could effectively penetrate the intestinal barrier and accumulate in the mouse liver. Importantly, these PS-NPs were found to be excreted from the liver after a certain recovery period.

3.3. Exposure to 100 nm PS-NPs induced a more pronounced non-alcoholic fatty liver disease (NAFLD)-like phenotype than exposure to 500 nm PS-NPs in mice

We next investigated the hepatotoxicity of 100 nm and 500 nm PS-NPs in mice. Fig. 3**A and B** showed that exposure to 100 nm PS-NPs for 180 days had more weight gain than the control group, accompanied by a significant increase of liver weight. For lipids, there was no distinct change in hepatic TC (Fig. S1), while hepatic TG was increased in mice exposed to 100 nm PS-NPs (Fig. 3**C**). In contrast to the effects observed in 100 nm PS-NPs-exposed group, no significant differences were detected in body weight, liver weight, and hepatic TG levels between 500 nm PS-NPs-exposed group and 180-day control group (Fig. 3**A-C**). Additionally, after 50 days of recovery, although the body weight and hepatic TG levels in the 100 nm-recovered group remained higher than those in the recovered control group (Fig. 3**A and C**), there was no significant change observed in liver weight (Fig. 3**B**). Oil-Red-O staining experiment further revealed that the accumulation of lipid droplets in the liver induced by 100 nm PS-NPs was more pronounced than that induced by 500 nm PS-NPs. Moreover, the area of lipid droplets was significantly reduced in the 100 nm PS-NPs-recovered group compared to the 100 nm-exposed group (Fig. 3**D and E**). Therefore, chronic dietary exposure to 100 nm PS-NPs resulted in a more pronounced effect on hepatic lipid accumulation in mice compared to 500 nm PS-NPs, and this effect was effectively alleviated after a certain period of recovery for 100 nm and 500 nm PS-NPs exposure.

3.4. Effect of PS-NPs exposure on lipid metabolism-related gene and protein expression in mice

To further confirm PS-NPs-induced hepatic lipid accumulation, the gene expression involved in lipid synthesis (Fig. 3**F,** Fig. S2**A-D**), uptake (Fig. 3**G,** Fig. S2**E-H**), oxidation (Fig. 3**H** and **I,** Fig. S2**I**) and secretion (Fig. 3**J,** Fig. S2**J** and **K**) were examined. Fig. 3**F** showed that the mRNA expression of *Srebf1* related to lipid synthesis was upregulated in the liver of 100 nm PS-NPs-exposed mice, compared to the 180-day control. Similarly, 100 nm PS-NPs exposure resulted in elevated expression of *Fabp1* (Fig. 3**G**). Moreover, the mRNA expression of *Acox1*, *Cpt1a*, and *Apoc3,* involved in lipid oxidation and secretion, was also increased in the liver of 100 nm PS-NPs-exposed mice (Fig. 3**H-J**). However, except for the upregulated *Srebf1*, the expression of *Fabp1*, *Acox1*, *Cpt1a*, and *Apoc3* did not change significantly in 500 nm PS-NPs-exposed group (Fig. 3**F-J**). After a 50-day recovery period, no significant differences were observed in the expression of 16 genes closely related to lipid metabolism in either the 100 nm PS-NPs-recovered group or the 500 nm PS-NPs-recovered group compared to the 230-day control group (Fig. 3**F-J,** Fig. S2**A-K**). To verify the changes of gene expression, the protein levels of Srebf1, Fabp1, Acox1, Cpt1a, and Apoc3 were further measured. Consistently, exposure to 100 nm PS-NPs led to an increase in the protein levels of Srebf1, Fabp1, Acox1, Cpt1a, and Apoc3 in mouse liver, all of which decreased after termination of exposure (Fig. 3**K,** Fig. S3**A-E**). For 500 nm PS-NPs-exposed group, there were no significant differences in the protein levels of Fabp1, Acox1, and Apoc3, while Srebf1 and Cpt1a was upregulated, and the fold change of Srebf1 and Cpt1a expression was less than that of the 100 nm PS-NPs-exposed group (Fig. 3**K,** Fig. S3**A-E**). Although the Cpt1a expression was still upregulated in 500 nm PS-NPs-recovered group, the Srebf1 expression was downregulated compared to the 500 nm PS-NPs-exposed group (Fig. 3**K,** Fig. S3**A, and** Fig. S3**D**). These results further indicated that 100 nm PS-NPs exhibited a greater potential to induce hepatic lipid accumulation than 500 nm PS-NPs at the molecular level, and this effect could be reversible.

3.5. PS-NPs exposure induced autophagosome formation, while simultaneously inhibiting autophagic degradation in mouse liver

Autophagy plays a crucial role in maintaining lipid homeostasis (Ueno and Komatsu, 2017; Scorletti and Carr, 2022). To elucidate the potential mechanism underlying PS-NPs-induced hepatic lipid accumulation, the changes of autophagic process in mouse liver were examined. Fig. 4**A** indicated that exposure to 100 nm PS-NPs resulted in excessive autophagosome formation, characterized by a marked increase in double-membrane-bound autophagic vacuoles. Moreover, the protein expression of Beclin 1 and ATG5, which was involved in the initiation and formation of autophagosomes, was evidently increased in response to 100 nm PS-NPs (Fig. 4**B-D**). Similarly, the expression of autophagosome formation marker protein LC3B II and the ratio of LC3B II/I were elevated (Fig. 4**B, E, and F**). These results suggested that 100 nm PS-NPs promoted the initiation and formation of hepatic autophagosomes in mice. Meanwhile, the inhibition of autophagic degradation was demonstrated by the increased protein expression of p62, an autophagic degradation marker protein, in the liver tissue of mice exposed to 100 nm PS-NPs (Fig. 4**B and G**). However, no statistically significant differences were observed in the LC3B II/I ratio and p62 protein

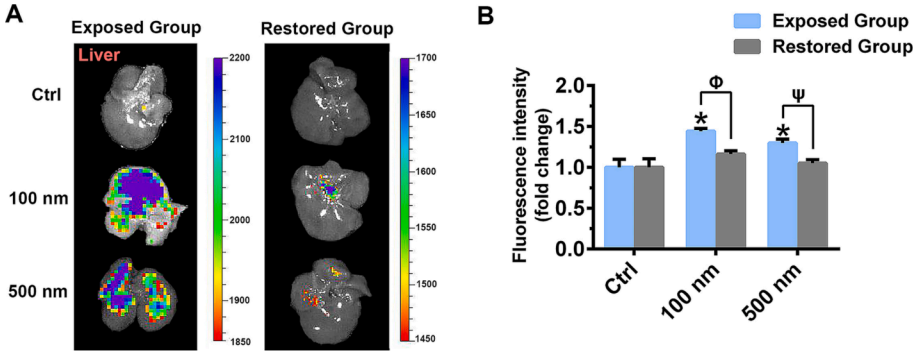

Fig. 2. Accumulation of fluorescent PS-NPs in mouse liver. (A) *Ex vivo* fluorescence imaging of the liver collected from the C57BL/6 mice drinking water with 100 nm and 500 nm fluorescent PS-NPs, respectively. (B) the fold change of total fluorescence intensity of the liver in the exposed groups and restored groups. the results were mean ± SEM (n = 5/group). *$p < 0.05$ the exposed group *vs.* the 180-day control; Φ$p < 0.05$ 100 nm PS-NPs-exposed group *vs.* 100 nm PS-NPs-restored group; ψ$p < 0.05$ 500 nm PS-NPs-exposed group *vs.* 500 nm PS-NPs-restored group.

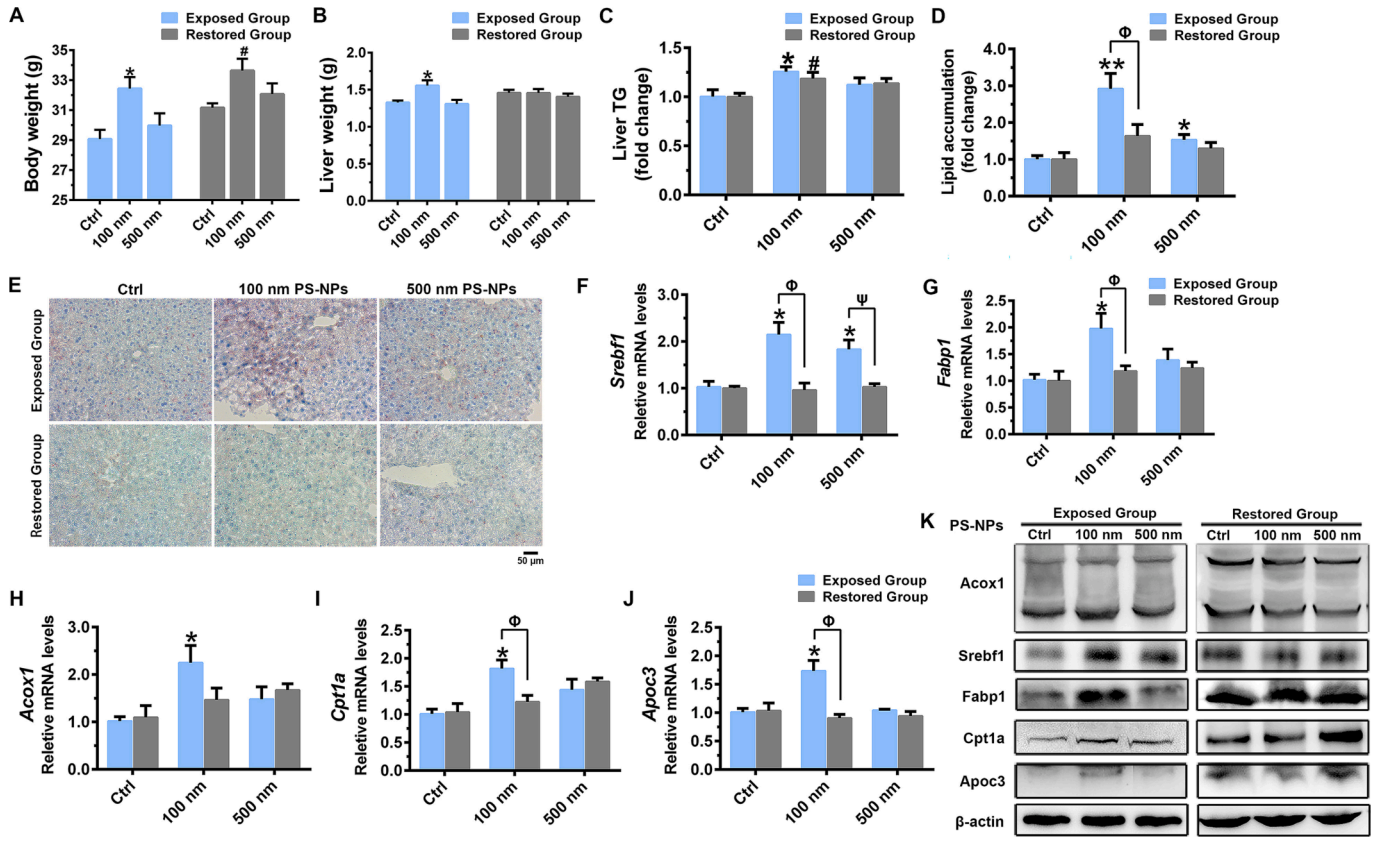

Fig. 3. Chronic dietary exposure to PS-NPs induced NAFLD-like phenotype in mice. (A) Body weight. (B) Liver weight. (C) the fold change of hepatic TG. (D) Lipid droplet area. (E) Representative images of liver section stained with Oil-red-O (scale bar, 50 μm). (F-J) the mRNA expression of *Srebf1*, *Fabp1*, *Acox1*, *Cpt1a*, and *Apoc3* in the exposed and restored groups (n = 5/group). (K) The protein expression of Srebf1, Fabp1, Acox1, Cpt1a, and Apoc3 in the exposed and restored groups. Data were mean ± SEM. $*p < 0.05$, $**p < 0.001$ the exposed group *vs.* the 180-day control; $\#p < 0.05$ the restored group *vs.* the 230-day control; $\Phi p < 0.05$, 100 nm PS-NPs-exposed group *vs.* 100 nm PS-NPs-restored group; $\psi p < 0.05$, 500 nm PS-NPs-exposed group *vs.* 500 nm PS-NPs-restored group. (For interpretation of the references to colour in this figure legend, the reader is referred to the web version of this article.)

expression between 500 nm PS-NPs-exposed group and 180-day control group; moreover, the fold changes of Beclin 1, ATG5, and LC3B II protein were relatively lower in the 500 nm PS-NPs-exposed group than those in the 100 nm PS-NPs-exposed group (Fig. 4**B-G)**. Additionally, the protein levels of Beclin 1, ATG5, LC3B II, and p62 were significantly reduced in the 100 nm and 500 nm PS-NPs-recovered groups compared to their corresponding exposed groups (Fig. 4**B-G)**, suggesting that autophagy dysregulation in mouse liver induced by 100 nm and 500 nm PS-NPs exposure were reversible.

3.6. PS-NPs exposure facilitated autophagosome formation via the ERK/mTOR signaling pathway

mTOR, mechanistic target of rapamycin kinase, serves as the central hub that manipulates autophagosome initiation and formation (Kim and Guan, 2015). Next, we analyzed the protein expression of mTOR in mouse liver. As expected, exposure to 100 nm and 500 nm PS-NPs inhibited the phosphorylation of mTOR (Fig. 5**A and B**). Correspondingly, the phosphorylation levels of ERK, a key upstream effector of mTOR, was also significantly reduced (Fig. 5**A and C**), suggesting that 100 nm and 500 nm PS-NPs might activate autophagosome initiation and formation through ERK/mTOR signaling pathway in mouse liver. Subsequently, after 50 days of recovery, the previously lowered phosphorylation levels of ERK and mTOR were restored to the levels comparable to those of the 230-day control (Fig. 5**A-C**).

3.7. PS-NPs exposure impaired lysosomal function in mice

The lysosomal function is essential to degrade the autophagic cargo. Fig. 6**A** demonstrated that a higher uptake of 100 nm PS-NPs by HepG2 cells was observed compared to 500 nm PS-NPs (green dots), and the internalized 100 nm PS-NPs were predominantly localized in lysosomes (yellow dots). Moreover, higher levels of lysosomal accumulation were observed in 100 nm PS-NPs-exposed cells compared to those exposed to 500 nm PS-NPs, as evidenced by changes in the number of yellow dots, the co-localization of red fluorescently labeled lysosomes with green fluorescently labeled PS-NPs. We thus speculated that 100 nm PS-NPs might cause more severe lysosomal damage than 500 nm PS-NPs. Indeed, the downregulation of Rab7 protein expression in the liver of mice exposed to 100 nm PS-NPs exhibited a greater magnitude compared to that in 500 nm PS-NPs-exposed group (Fig. 6**B and C**). Similarly, the lysosomal major hydrolytic proteases CTSB and CTSD were significantly downregulated in 100 nm PS-NPs-exposed group, but not in 500 nm PS-NPs-exposed group (Fig. 6**B, D and E**). These findings suggested that 100 nm PS-NPs caused more severe damage to lysosomes than 500 nm PS-NPs *in vivo*. Additionally, the internalized 100 nm and 500 nm PS-NPs predominantly accumulated in the lysosomes in HepG2 cells (Fig. 6**A**), suggesting a potential excretion pathway through lysosome-dependent exocytosis. To test this hypothesis, we employed ionomycin to stimulate lysosome-membrane fusion and bafilomycin A1 to inhibit lysosomal acidification. Fig. 6**F** showed that intracellular fluorescence intensity was decreased in the 100 nm PS-NPs + ionomycin group, whereas it was increased in the 100 nm PS-NPs + bafilomycin A1 group compared to the 100 nm PS-NPs group. Similar changes were also

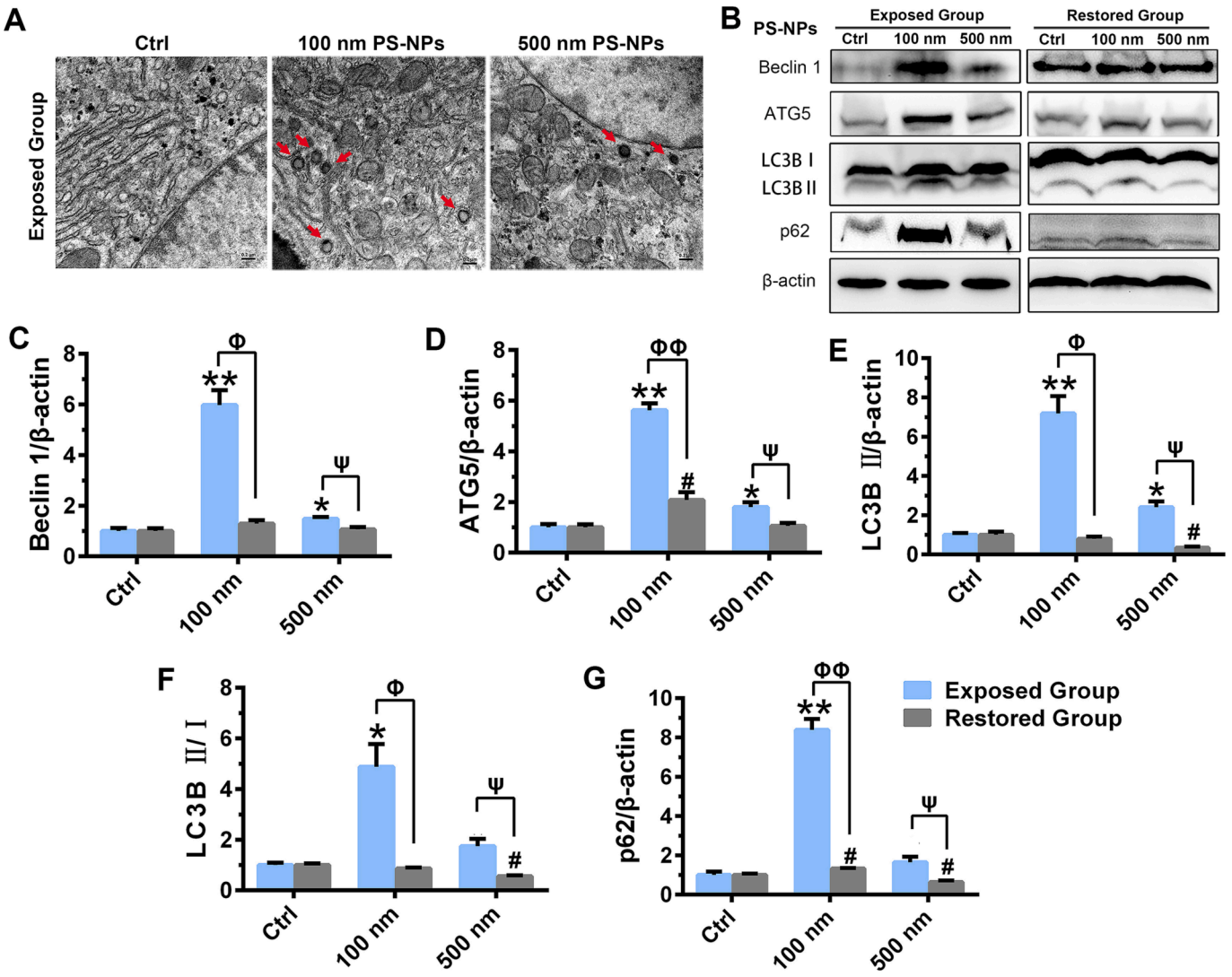

Fig. 4. Size-dependent effects and reversibility of the autophagosome formation and autophagic degradation induced by PS-NPs in mice. (A) Representative images of liver sections detected by the TEM in exposed groups (magnification, ×30,000). The red arrows indicate autophagosomes. (B) The protein expression of ATG5, Beclin 1, LC3B, and p62. (C-G) Quantification of the protein levels of Beclin 1, ATG5, LC3B II, LC3B II/LC3B I, and p62 (n = 5/group). Data were mean ± SEM. *$p < 0.05$, **$p < 0.001$ the exposed group *vs.* the 180-day control; #$p < 0.05$ the restored group *vs.* the 230-day control; Φ$p < 0.05$, ΦΦ$p < 0.001$ 100 nm PS-NPs-exposed group *vs.* 100 nm PS-NPs-restored group; ψ$p < 0.05$ 500 nm PS-NPs-exposed group *vs.* 500 nm PS-NPs-restored group. (For interpretation of the references to colour in this figure legend, the reader is referred to the web version of this article.)

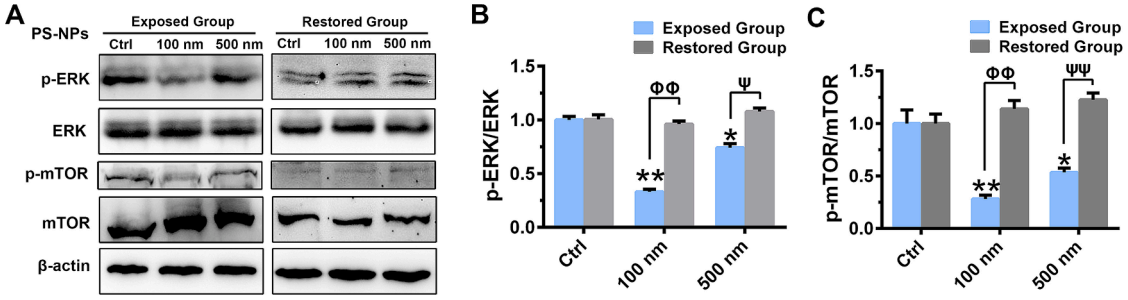

Fig. 5. Effect of chronic dietary exposure to PS-NPs on the ERK/mTOR pathway in mouse liver. (A) The protein expression of ERK, p-ERK, mTOR, and p-mTOR in the exposed groups and restored groups. (B and C) Quantification of the protein levels of p-ERK/ERK and p-mTOR/mTOR. Data were mean ± SEM (n = 5/group). *$p < 0.05$, **$p < 0.001$ the exposed group *vs.* the 180-day control; ΦΦ$p < 0.001$ 100 nm PS-NPs-exposed group *vs.* 100 nm PS-NPs-restored group; ψ$p < 0.05$, ψψ$p < 0.001$ 500 nm PS-NPs-exposed group *vs.* 500 nm PS-NPs-restored group.

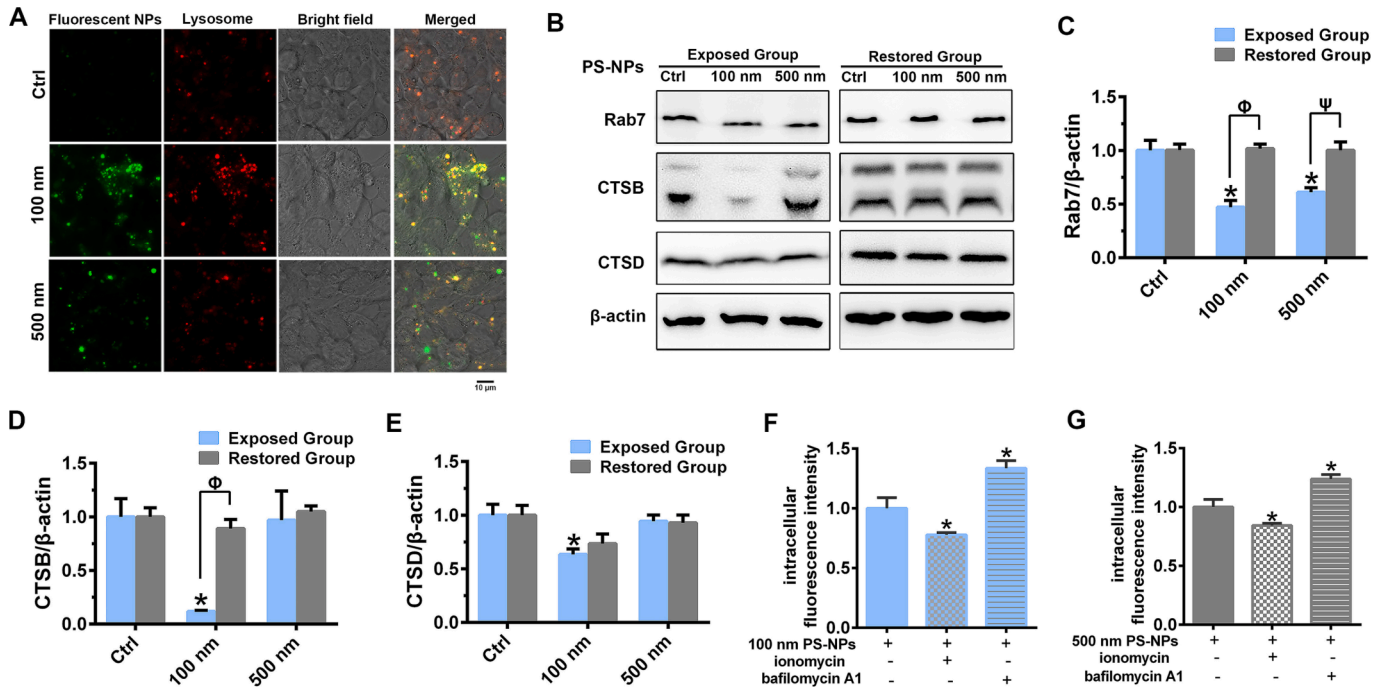

Fig. 6. Effect of PS-NPs exposure on lysosomal function. (A) Localization of fluorescent PS-NPs in HepG2 cells. Lysosomes were stained with LysoTracker Red DND-99, and PS-NPs with the size of 100 nm and 500 nm were filled with green fluorescent substances. The yellow (red^{+} green^{+}) puncta showed the overlap of PS-NPs and lysosomes from the merged micrographs (scale bar, 10 μm). (B) The protein expression of Rab7, CTSB, and CTSD in the exposed groups and restored groups. (C-E) Quantification of the protein levels of Rab7, CTSB, and CTSD (n = 5/group). (F) Intracellular fluorescence intensity using ionomycin or bafilomycin A1 co-treated with 100 nm PS-NPs. (G) Intracellular fluorescence intensity using ionomycin or bafilomycin A1 co-treated with 500 nm PS-NPs. Data were mean ± SEM. *$p < 0.05$ the exposed group *vs.* the 180-day control; Φ$p < 0.05$ 100 nm PS-NPs-exposed group *vs.* 100 nm PS-NPs-restored group; ψ$p < 0.05$ 500 nm PS-NPs-exposed group *vs.* 500 nm PS-NPs-restored group. (For interpretation of the references to colour in this figure legend, the reader is referred to the web version of this article.)

observed in the 500 nm PS-NPs + ionomycin group and the 500 nm PS-NPs + bafilomycin A1 group (Fig. 6**G**). These findings confirmed that the lysosomal exocytosis was an important route for cellular clearance of both 100 nm and 500 nm PS-NPs in HepG2 cells. Furthermore, it is noteworthy that the protein expression of Rab7, CTSB, and CTSD returned to comparable levels with those of the 230-day control after a 50-day recovery period in both 100 nm and 500 nm PS-NPs-recovered groups (Fig. 6**B-E**).

4. Discussion

The ubiquitous NMPs in the natural environment inevitably increase human exposure risks, and recent studies have detected the presence of NMPs in human liver tissue, highlighting the practical significance of studying their hepatotoxicity (Cox et al., 2019; Vethaak and Legler, 2021; Horvatits et al., 2022; Leslie et al., 2022). However, little information is currently available regarding potential hazards posed by NMPs to hepatic lipid accumulation and related molecular mechanisms. In this study, we clarified the size-dependent effect of PS-NPs-induced lipid accumulation at an environmentally relevant dose in mice, which was associated with abnormal autophagy and lysosomal damage. More importantly, we revealed for the first time that PS-NPs accumulated in the liver could be excreted from the body and the effects of lipid accumulation could be alleviated upon termination of PS-NPs exposure.

In this study, fluorescent PS-NPs with particle sizes of 100 nm and 500 nm were observed in the mouse liver through *ex vivo* fluorescence imaging. Consistently, these two particle sizes of PS-NPs could accumulate in the liver of Nile tilapia (*Oreochromis niloticus*) determined using the pyrolysis method in combination with gas chromatography-mass spectrometry (Py-GC/MS) (Wang et al., 2023). It's worth noting that Yu et al. (2019) verified that NPs were predominantly distributed in the liver, followed by the spleen and lung tissues in mice. Similarly, Gao et al. (2022) also confirmed that mice exposed to polyethylene terephthalate (PET) NPs showed the highest accumulation of NPs in their liver compared to other organs, with NPs concentrations 7-fold higher than those detected in the spleen, the second organ where NPs accumulated. Thus, it is of substantial scientific significance to evaluate NPs-induced hepatotoxicity. Considering that the liver is one of the largest metabolic organs in the organism and plays a pivotal role in lipid metabolism, we focused on investigating the effect of PS-NPs accumulated in the liver on lipid metabolism *in vivo*. Our results showed that oral exposure to environmentally equivalent concentrations of 100 nm and 500 nm PS-NPs for 180 days resulted in the excessive accumulation of lipid droplets in the liver of mice. Furthermore, the impact of 100 nm PS-NPs on lipid accumulation was significantly more pronounced than that of 500 nm PS-NPs. This particle size-dependent effect was also verified by the gene and protein trends of Srebf1, Fabp1, Acox1, Cpt1a, and Apoc3 following exposure to 100 nm and 500 nm PS-NPs. Although the effect of 500 nm PS-NPs exposure on lipid metabolism was inferior to that of 100 nm PS-NPs, there was still a slight induction of lipid accumulation and a significant upregulation of Srebf1 and Cpt1a. Conversely, a previous study reported negative regulation of lipid metabolism after exposure to 500 nm PS-NPs, as evidenced by decreased TG levels and reduced gene expression involved in TG synthesis (Lu et al., 2018). The reason for such differential outcomes might be due to the effect of exposure duration on lipid metabolism, which was 35 days in this previous study compared to 180 days in ours. Long-term exposure to NMPs has been found to induce obesity and lipid accumulation in other laboratory animal models, such as marine medaka (*Oryzias melastigma*) and chickens (Zhang et al., 2021a; Yin et al., 2023). In a mouse model, Shi et al. (2022) found that exposure to 1 μm PS MPs resulted in significant differences in cortisol, acetylcholine, and N-Acetyl-D-Glucosamine (GlcNAc) levels determining by metabolome analysis. These changes increased the risks of insulin resistance, which was one of the most critical mechanisms involved in lipid metabolism interference and adipogenesis promotion. When the exposed particle size was

reduced to approximately 60 nm, NPs exposure did accelerate lipid accumulation in the liver (Shiu et al., 2022). Similarly, Cheng et al. (2022) confirmed that exposure to 1 μm PS MPs increased the lipid accumulation and TG contents in the liver organoids *in vitro*, even at a low concentration of 0.25 μg/mL. Collectively, although NMPs are considered inert polymers, their potential hepatotoxicity and impact on lipid metabolism cannot be disregarded. Our findings, together with most previous studies, suggested that long-term exposure to NMPs could induce hepatic lipid accumulation, which was closely related to the particle size.

Mechanistically, limited research suggested that NMPs-induced disruption of lipid metabolism was associated with gut microbiota dysbiosis, increased gut permeability, and inflammation (Lu et al., 2018; Deng et al., 2022). Notably, autophagy has emerged as an important mechanism in the biotoxicity induced by environmental pollutants such as airborne particulate matter, nanomaterials, and certain common single environmental chemicals over the past decade (Stern et al., 2012; Popp and Segatori, 2015; Pesonen and Vähäkangas, 2019). In toxicity studies of NMPs, abnormal autophagy has been also observed *in vivo* in tissues such as liver, kidney, brain, and testis (Wang et al., 2021b; Yin et al., 2022; Zhong et al., 2022; Zhou et al., 2022). It has been reported that activated ERK can directly or indirectly activate the mTORC1 complex to negatively regulate the initiation and formation of autophagosomes (Ma et al., 2005; Carrière et al., 2008; Carriere et al., 2011; Wang et al., 2019). Likewise, in this study, oral exposure to environmentally relevant doses of 100 nm and 500 nm PS-NPs for 180 days promoted autophagosome formation through inhibition of the ERK/mTOR signaling pathway. However, autophagic degradation was inhibited, as evidenced by an increase in p62 protein expression in the PS-NPs-exposed group. Throughout the autophagic process, autophagosomes are delivered to lysosomes for subsequent fusion events. Within the acidic microenvironment of lysosomes, the contents encapsulated in autophagosomes are degraded by hydrolytic enzymes. Therefore, maintaining structural and functional integrity of lysosomes is critical for the successful autophagic degradation (Yamamoto et al., 2023). In this study, we further verified that 100 nm and 500 nm PS-NPs were accumulated in lysosomes in HepG2 cells *in vitro*, and the expression of lysosomal hydrolytic proteases CTSB and CTSD was inhibited in mouse liver. These findings suggested lysosomal function was impaired in the PS-NPs-exposed groups, which might account for the impaired autophagic flux induced by PS-NPs. Notably, the degree of lysosomal impairment exhibited a strong correlation with the size of PS-NPs, as evidenced by the lower expression levels of Rab7, CTSB, and CTSD in the 100 nm PS-NPs-exposed group compared to those in the 500 nm PS-NPs-exposed group.

Emerging evidence has confirmed the crucial physiological role of autophagy in lipid metabolism, particularly in the degradation of lipid droplets (Singh et al., 2009). This selective autophagy process was also known as lipophagy. Dysfunctions or overloading of lipophagy were strongly implicated in the pathogenesis of NAFLD (Zhang et al., 2021b). For instance, Bisphenol F (BPF), a primary substitute for BPA, inhibited lysosomal degradative capacity, thereby contributing to lipophagic disorder and inducing lipid droplet deposition (Wang et al., 2021a). This study highlighted the important role of lysosomal events in the process of lipophagy. The small GTPase Rab7, a marker protein of the late endocytic pathway, was indispensable for hepatic lipophagy as it involved in autophagosome-lysosome fusion and facilitated the trafficking of lysosomes to lipid droplets. Inhibition of Rab7 resulted in morphological alterations of lysosomes and autophagosomes, consequently impaired the ability to breakdown lipid droplets (Schroeder et al., 2015). In this study, the protein expression of Rab7 was reduced in the PS-NPs-exposed groups, suggesting that 100 nm and 500 nm PS-NPs inhibited the fusion of autophagosomes with lysosomes, which in turn might alleviate the breakdown of lipid droplets and cause excessive lipid accumulation. A previous study suggested that the decreased activities of cathepsins regulated lipid metabolism in murine steatohepatitis (Houben et al., 2017). This also supported our speculation that 100 nm PS-NPs-induced downregulation in CTSB and CTSD expression promoted lipid droplet deposition. Collectively, it was reasonable to conclude that exposure to PS-NPs resulted in impaired lysosomal function and dysfunction of autophagosome and lysosome fusion, thereby inhibiting autophagic flux and contributing to hepatic lipid accumulation in mice. Furthermore, this effect was observed to be particle size-dependent, with 100 nm PS-NPs exhibiting a more pronounced autophagy-dependent lipid accumulation compared to 500 nm PS-NPs.

The biodistribution and toxicity of particles in living organisms are determined by several factors, including particle size, material composition, surface charge, and hydrophobicity/hydrophilicity (Roshanzadeh et al., 2020; Stock et al., 2021; Banerjee et al., 2022; Du et al., 2023). Among these factors, particle size is regarded as one of the most influential determinants. In the mouse model, no significant accumulation of NMPs with a particle size larger than 40 μm was observed in the intestine or liver (Deng et al., 2022); however, NMPs smaller than 20 μm were detected in the liver, kidney, and intestine of mice (Deng et al., 2017). Moreover, the bioavailability of NMPs was observed to increase as particle size decreased. Liang et al. (2021) demonstrated higher accumulation of 50 nm PS NMPs compared to 500 nm and 5000 nm PS NMPs in various organs of mice, including intestine, liver, kidney, brain, heart, lungs, spleen, testis, and epididymis. The total bioavailability for 50 nm, 500 nm and 5000 nm PS NMPs were found to be 6.16 %, 1.53 % and 0.46 %, respectively. Regarding the biodistribution of nanoplastics with particle sizes of 100 nm and 500 nm, Wang et al. (2023) also verified that 100 nm PS-NPs exhibited significantly higher accumulation than 500 nm PS-NPs in the liver of Nile tilapia (*Oreochromis niloticus*), resulting in particle size-dependent hepatic steatosis. Consistently, in this study, higher accumulation of PS-NPs was observed in HepG2 cells for 100 nm particles compared to 500 nm ones (green dots, Fig. 6**A**); more importantly, 100 nm PS-NPs induced more severe lysosomal damage and more pronounced blockage of autophagic flux in mice, which was closely associated with the degradation of lipid droplets. These findings elucidate the potential mechanisms underlying the size-dependent effect of PS-NPs on hepatic lipid accumulation.

Nano/microplastics are a distinct category of solid pollutants that exhibit chemical inertness and resistance to degradation under mild conditions, raising questions about their potential for excretion in organisms and the possibility of spontaneous recovery from induced toxicity. In this study, 100 nm and 500 nm PS-NPs accumulated in the liver of mice were significantly decreased after a period of recovery, suggesting internalized PS-NPs could be excreted from the body via specific exocytosis pathway. Lysosomal exocytosis is an important pathway for cellular clearance and tissue remodeling, which involves the fusion of lysosomes with the plasma membrane, resulting in the elimination of lysosomal contents (Sakhtianchi et al., 2013; Buratta et al., 2020). A recent study found that 50 nm and 500 nm PS-NPs were mainly accumulated in lysosomes after being taken up by rat basophilic leukemia (RBL-2H3) cells, subsequently undergoing excretion through energy-dependent lysosomal exocytosis and energy-free penetration (Liu et al., 2021). Similarly, in this study, the majority of PS-NPs uptake by HepG2 cells were localized in lysosomes, particularly those with a small particle size of 100 nm. These PS-NPs could be excreted from the cells via lysosomal pathway, suggesting that PS-NPs accumulated in mouse liver were most likely to undergo lysosomal exocytosis for elimination. More importantly, the effect of PS-NPs on hepatic lipid accumulation and autophagy was completely reversed and even restored to comparable levels in the control group following a self-recovery period of 50 days in mice. These findings provide evidence that lysosomes, which are involved in the cellular exocytosis pathway, may play a crucial role in both the elimination of PS-NPs and tissue repair.

In vivo studies have demonstrated that the liver is one of the most important target organs for the accumulation and toxic effects of NMPs, and the presence of NMPs has been detected in human liver samples

(Horvatits et al., 2022). Previous toxicological studies mainly investigated the hepatic inflammation, oxidative stress, and apoptosis induced by NMPs exposure (Li et al., 2021b; Banerjee et al., 2022). Notably, in recent years, the autophagy-lysosome pathway has begun to receive increasing attention as an emerging mechanism in disturbing hepatic lipid metabolism and exacerbating the progression of NAFLD (Singh et al., 2009; Scorletti and Carr, 2022). Moreover, lysosomes, as terminal degradative organelles, are directly involved in the process of autophagic flux and play an important role in environmental pollutants-induced lipid accumulation (Song et al., 2019; Wang et al., 2021a; Zhao et al., 2022). However, the involvement of lysosomes in NPs-induced hepatotoxicity has not yet been reported. In this study, exposure to 100 nm and 500 nm PS-NPs impaired the degradative capacity of lysosomes, thereby inhibiting autophagic flux and contributing to hepatic lipid accumulation in mice. On the other hand, lysosomal exocytosis is an important cellular clearance mechanism, involving the fusion of lysosomes with the plasma membrane for extracellular release (Sakhtianchi et al., 2013; Buratta et al., 2020). This process plays a critical role in maintaining cellular fitness and promoting tissue remodeling. In this study, we also discovered for the first time that 100 nm and 500 nm PS-NPs could be excreted from the body via lysosomal exocytosis and alleviate the inhibition of autophagic flux, thus facilitating the breakdown of lipid droplets during self-recovery. Collectively, this dual function of lysosomes deserves particular attention for their potential implications in both autophagy-dependent lipid accumulation and exocytosis pathway triggered by NPs. Targeting the lysosomes to restore normal lysosomal function and autophagy is a promising strategy for treating NPs-induced hepatic lipid accumulation.

5. Conclusions

Our findings offer a novel perspective for understanding the hepatotoxicity of environmentally relevant doses of NPs exposure on terrestrial mammals. The special characteristics of NPs, including their diverse particle sizes and stable chemical inertness, lead to the complexity and uncertainty of their toxicological effects. In this study, long-term oral exposure to an environmentally relevant dose of 100 nm and 500 nm PS-NPs induced hepatic lipid accumulation in mice, and this effect was more pronounced in 100 nm PS-NPs-exposed group than in 500 nm PS-NPs-exposed group, potentially due to size-dependent blockage of autophagic flux. Notably, we also found for the first time that 100 nm and 500 nm PS-NPs-induced lipid accumulation was reversible and self-restoring after termination of exposure. More importantly, lysosomes play a crucial role in the process of PS-NPs exposure and subsequent self-recovery. Exposure to 100 nm and 500 nm PS-NPs impaired lysosomal function, thereby inhibiting the autophagic degradation, and contributing to lipid accumulation. After termination of PS-NPs exposure, lysosomes participated in the exocytosis pathway of PS-NPs excretion, thus facilitating the restoration of impaired autophagic flux and the breakdown of lipid droplets. This dual function of lysosomes in the liver injury and repair induced by nanoplastics exposure deserves further attention.

Funding

This work was financially supported by the National Natural Science Foundation of China [42007387 and 22076179], and the Natural Science Foundation of Fujian Province, China [2023J01224 and 2022J06033].

CRediT authorship contribution statement

Yan-Yang Lu: Writing – review & editing, Writing – original draft, Methodology, Investigation, Funding acquisition, Data curation, Conceptualization, Writing – review & editing, Funding acquisition. **Lu Lu:** Writing – review & editing, Methodology. **Hong-Yun Ren:** Methodology. **Weizhen Hua:** Methodology. **Nengxing Zheng:** Methodology. **Fu-Yi Huang:** Methodology. **Jiani Wang:** Methodology. **Meiping Tian:** Methodology. **Qingyu Huang:** Writing – review & editing, Funding acquisition.

Declaration of competing interest

The authors declare that they have no known competing financial interests or personal relationships that could have appeared to influence the work reported in this paper.

Data availability

Data will be made available on request.

Appendix A. Supplementary data Hepatic TC content (Fig. S1); Expression of genes involved in lipid synthesis, uptake, oxidation, and secretion (Fig. S2); Quantification of the protein levels of Srebf1, Fabp1, Acox1, Cpt1a, and Apoc3 (Fig. S3).

Supplementary data to this article can be found online at https://doi.org/10.1016/j.envint.2024.108532.

References

Banerjee, A., Billey, L.O., McGarvey, A.M., Shelver, W.L., 2022. Effects of polystyrene micro/nanoplastics on liver cells based on particle size, surface functionalization, concentration and exposure period. Sci. Total Environ. 836, 155621.
Buratta, S., Tancini, B., Sagini, K., Delo, F., Chiaradia, E., Urbanelli, L., Emiliani, C., 2020. Lysosomal exocytosis, exosome release and secretory autophagy: the autophagic- and Endo-lysosomal systems go extracellular. Int. J. Mol. Sci. 21 (7), 2576.
Carrière, A., Cargnello, M., Julien, L.A., Gao, H., Bonneil, E., Thibault, P., Roux, P.P., 2008. Oncogenic MAPK signaling stimulates mTORC1 activity by promoting RSK-mediated raptor phosphorylation. Curr. Biol. 18, 1269–1277.
Carriere, A., Romeo, Y., Acosta-Jaquez, H.A., Moreau, J., Bonneil, E., Thibault, P., Fingar, D.C., Roux, P.P., 2011. ERK1/2 phosphorylate raptor to promote ras-dependent activation of mTOR complex 1 (mTORC1). J. Biol. Chem. 286, 567–577.
Chen, X., Zhuang, J., Chen, Q., Xu, L., Yue, X., Qiao, D., 2022. Chronic exposure to polyvinyl chloride microplastics induces liver injury and gut microbiota dysbiosis based on the integration of liver transcriptome profiles and full-length 16S rRNA sequencing data. Sci. Total Environ. 839, 155984.
Cheng, W., Li, X., Zhou, Y., Yu, H., Xie, Y., Guo, H., Wang, H., Li, Y., Feng, Y., Wang, Y., 2022. Polystyrene microplastics induce hepatotoxicity and disrupt lipid metabolism in the liver organoids. Sci. Total Environ. 806, 150328.
Cox, K.D., Covernton, G.A., Davies, H.L., Dower, J.F., Juanes, F., Dudas, S.E., 2019. Human consumption of microplastics. Environ. Sci. Technol. 53, 7068–7074.
Deng, Y., Zhang, Y., Lemos, B., Ren, H., 2017. Tissue accumulation of microplastics in mice and biomarker responses suggest widespread health risks of exposure. Sci. Rep. 7, 46687.
Deng, Y., Chen, H., Huang, Y., Zhang, Y., Ren, H., Fang, M., Wang, Q., Chen, W., Hale, R. C., Galloway, T.S., Chen, D., 2022. Long-term exposure to environmentally relevant doses of large polystyrene microplastics disturbs lipid homeostasis via bowel function interference. Environ. Sci. Technol. 56, 15805–15817.
Ding, L., Yao, C., Yin, X., Li, C., Huang, Y., Wu, M., Wang, B., Guo, X., Wang, Y., Wu, M., 2018. Size, shape, and protein Corona determine cellular uptake and removal mechanisms of gold nanoparticles. Small 14, e1801451.
Du, T., Yu, X., Shao, S., Li, T., Xu, S., Wu, L., 2023. Aging of nanoplastics significantly affects protein Corona composition thus enhancing macrophage uptake. Environ. Sci. Technol. 57, 3206–3217.
Fan, Y., Lu, J., Liu, J., Zhang, R., Yu, Z., Guan, S., 2021. 1,3-dichloro-2-propanol induced hepatic lipid accumulation by inhibiting autophagy via AKT/mTOR/FOXO1 pathway in mice. Food Chem. Toxicol. 157, 112578.
Gao, Q., Wang, Y., Ji, Y., Zhao, X., Zhang, P., Chen, L., 2022. Tracking of realistic nanoplastics in complicated matrices by iridium element labeling and inductively coupled plasma mass spectroscopy. J. Hazard Mater. 424, 127628.
Geyer, R., Jambeck, J.R., Law, K.L., 2017. Production, use, and fate of all plastics ever made. Sci. Adv. 3, e1700782.
Gigault, J., Halle, A.T., Baudrimont, M., Pascal, P.Y., Gauffre, F., Phi, T.L., El Hadri, H., Grassl, B., Reynaud, S., 2018. Current opinion: what is a nanoplastic? Environ. Pollut. 235, 1030–1034.
Gonçalves, J.M., Bebianno, M.J., 2021. Nanoplastics impact on marine biota: a review. Environ. Pollut. 273, 116426.
Han, M., Zhu, C., Tang, S., Liang, J., Li, D., Guo, Y., Zuraini, Z., Si, Q., Jiang, Q., 2023. The effects of a polystyrene nanoplastic on the immune response and gut microbiota of Eriocheir sinensis and its post-recovery state. Aquat. Toxicol. 262, 106644.

Horvatits, T., Tamminga, M., Liu, B., Sebode, M., Carambia, A., Fischer, L., Püschel, K., Huber, S., Fischer, E.K., 2022. Microplastics detected in cirrhotic liver tissue. EBioMedicine 82, 104147.
Houben, T., Oligschlaeger, Y., Hendrikx, T., Bitorina, A.V., Walenbergh, S.M.A., van Gorp, P.J., Gijbels, M.J.J., Friedrichs, S., Plat, J., Schaap, F.G., Lütjohann, D., Hofker, M.H., Shiri-Sverdlov, R., 2017. Cathepsin D regulates lipid metabolism in murine steatohepatitis. Sci. Rep. 7, 3494.
Huang, Y., Wong, K.K., Li, W., Zhao, H., Wang, T., Stanescu, S., Boult, S., van Dongen, B., Mativenga, P., Li, L., 2022. Characteristics of nano-plastics in bottled drinking water. J. Hazard. Mater. 424, 127404.
Kim, Y.C., Guan, K.L., 2015. mTOR: a pharmacologic target for autophagy regulation. J. Clin. Invest. 125, 25–32.
Klein, M., Fischer, E.K., 2019. Microplastic abundance in atmospheric deposition within the metropolitan area of Hamburg, Germany. Sci. Total Environ. 685, 96–103.
Klionsky, D.J., Abdalla, F.C., Abeliovich, H., Abraham, R.T., Acevedo-Arozena, A., Adeli, K., Agholme, L., Agnello, M., Agostinis, P., Aguirre-Ghiso, J.A., et al., 2012. Guidelines for the use and interpretation of assays for monitoring autophagy. Autophagy 8, 445–544.
Leslie, H.A., van Velzen, M.J.M., Brandsma, S.H., Vethaak, A.D., Garcia-Vallejo, J.J., Lamoree, M.H., 2022. Discovery and quantification of plastic particle pollution in human blood. Environ. Int. 163, 107199.
Li, L., Gu, H., Chang, X., Huang, W., Sokolova, I.M., Wei, S., Sun, L., Li, S., Wang, X., Hu, M., Zeng, J., Wang, Y., 2021a. Oxidative stress induced by nanoplastics in the liver of juvenile large yellow croaker Larimichthys crocea. Mar. Pollut. Bull. 170, 112661.
Li, S., Ma, Y., Ye, S., Tang, S., Liang, N., Liang, Y., Xiao, F., 2021b. Polystyrene microplastics trigger hepatocyte apoptosis and abnormal glycolytic flux via ROS-driven calcium overload. J. Hazard. Mater. 417, 126025.
Liang, B., Zhong, Y., Huang, Y., Lin, X., Liu, J., Lin, L., Hu, M., Jiang, J., Dai, M., Wang, B., Zhang, B., Meng, H., Lelaka, J.J.J., Sui, H., Yang, X., Huang, Z., 2021. Underestimated health risks: polystyrene micro- and nanoplastics jointly induce intestinal barrier dysfunction by ROS-mediated epithelial cell apoptosis. Part. Fibre Toxicol. 18, 20.
Liu, L., Xu, K., Zhang, B., Ye, Y., Zhang, Q., Jiang, W., 2021. Cellular internalization and release of polystyrene microplastics and nanoplastics. Sci. Total Environ. 779, 146523.
Lu, L., Wan, Z., Luo, T., Fu, Z., Jin, Y., 2018. Polystyrene microplastics induce gut microbiota dysbiosis and hepatic lipid metabolism disorder in mice. Sci. Total Environ. 631–632, 449–458.
Ma, L., Chen, Z., Erdjument-Bromage, H., Tempst, P., Pandolfi, P.P., 2005. Phosphorylation and functional inactivation of TSC2 by erk implications for tuberous sclerosis and cancer pathogenesis. Cell 121, 179–193.
Nair, A.B., Jacob, S., 2016. A simple practice guide for dose conversion between animals and human. J. Basic Clin. Pharm. 7, 27–31.
Pesonen, M., Vähäkangas, K., 2019. Autophagy in exposure to environmental chemicals. Toxicol. Lett. 305, 1–9.
Popp, L., Segatori, L., 2015. Differential autophagic responses to nano-sized materials. Curr. Opin. Biotechnol. 36, 129–136.
Roshanzadeh, A., Park, S., Ganjbakhsh, S.E., Park, J., Lee, D.H., Lee, S., Kim, E.S., 2020. Surface charge-dependent cytotoxicity of plastic nanoparticles in alveolar cells under cyclic stretches. Nano Lett. 20, 7168–7176.
Sakhtianchi, R., Minchin, R.F., Lee, K.B., Alkilany, A.M., Serpooshan, V., Mahmoudi, M., 2013. Exocytosis of nanoparticles from cells: role in cellular retention and toxicity. Adv. Colloid Interface Sci. 201–202, 18–29.
Samandra, S., Mescall, O.J., Plaisted, K., Symons, B., Xie, S., Ellis, A.V., Clarke, B.O., 2022. Assessing exposure of the australian population to microplastics through bottled water consumption. Sci. Total Environ. 837, 155329.
Schroeder, B., Schulze, R.J., Weller, S.G., Sletten, A.C., Casey, C.A., McNiven, M.A., 2015. The small GTPase Rab7 as a central regulator of hepatocellular lipophagy. Hepatology 61, 1896–1907.
Scorletti, E., Carr, R.M., 2022. A new perspective on NAFLD: focusing on lipid droplets. J. Hepatol. 76, 934–945.
Senathirajah, K., Attwood, S., Bhagwat, G., Carbery, M., Wilson, S., Palanisami, T., 2021. Estimation of the mass of microplastics ingested - a pivotal first step towards human health risk assessment. J. Hazard. Mater. 404, 124004.
Shi, C., Han, X., Guo, W., Wu, Q., Yang, X., Wang, Y., Tang, G., Wang, S., Wang, Z., Liu, Y., Li, M., Lv, M., Guo, Y., Li, Z., Li, J., Shi, J., Qu, G., Jiang, G., 2022. Disturbed gut-liver axis indicating oral exposure to polystyrene microplastic potentially increases the risk of insulin resistance. Environ. Int. 164, 107273.
Shi, C., Liu, Z., Yu, B., Zhang, Y., Yang, H., Han, Y., Wang, B., Liu, Z., Zhang, H., 2023. Emergence of nanoplastics in the aquatic environment and possible impacts on aquatic organisms. Sci. Total Environ. 906, 167404.
Shiu, H.T., Pan, X., Liu, Q., Long, K., Cheng, K.K.Y., Ko, B.C., Fang, J.K., Zhu, Y., 2022. Dietary exposure to polystyrene nanoplastics impairs fasting-induced lipolysis in adipose tissue from high-fat diet fed mice. J. Hazard. Mater. 440, 129698.
Singh, R., Kaushik, S., Wang, Y., Xiang, Y., Novak, I., Komatsu, M., Tanaka, K., Cuervo, A. M., Czaja, M.J., 2009. Autophagy regulates lipid metabolism. Nature 458, 1131–1135.
Song, D., Chen, Y., Wang, B., Li, D., Xu, C., Huang, H., Huang, S., Liu, R., 2019. Bisphenol a inhibits autophagosome-lysosome fusion and lipid droplet degradation. Ecotoxicol. Environ. Saf. 183, 109492.
Stern, S.T., Adiseshaiah, P.P., Crist, R.M., 2012. Autophagy and lysosomal dysfunction as emerging mechanisms of nanomaterial toxicity. Part. Fibre Toxicol. 9, 20.
Stock, V., Laurisch, C., Franke, J., Dönmez, M.H., Voss, L., Böhmert, L., Braeuning, A., Sieg, H., 2021. Uptake and cellular effects of PE, PP, PET and PVC microplastic particles. Toxicol. in Vitro 70, 105021.
Ueno, T., Komatsu, M., 2017. Autophagy in the liver: functions in health and disease. Nat. Rev. Gastroenterol. Hepatol. 14, 170–184.
UNEP, 2021. From Pollution to Solution: A Global Assessment of Marine Litter and Plastic Pollution. https://www.grida.no/publications/747.
Van Cauwenberghe, L., Janssen, C.R., 2014. Microplastics in bivalves cultured for human consumption. Environ. Pollut. 193, 65–70.
Vethaak, A.D., Legler, J., 2021. Microplastics and human health. Science 371, 672–674.
Wang, H., Liu, Y., Wang, D., Xu, Y., Dong, R., Yang, Y., Lv, Q., Chen, X., Zhang, Z., 2019. The Upstream Pathway of mTOR-Mediated Autophagy in Liver Diseases. Cells 8, 1597.
Wang, Y.L., Lee, Y.H., Hsu, Y.H., Chiu, I.J., Huang, C.C., Huang, C.C., Chia, Z.C., Lee, C. P., Lin, Y.F., Chiu, H.W., 2021b. The kidney-related effects of polystyrene microplastics on human kidney proximal tubular epithelial cells HK-2 and male C57BL/6 mice. Environ. Health. Perspect. 129, 57003.
Wang, W., Mao, X., Zhang, R., Zhou, X.X., Liu, Y., Zhou, H., Jia, J., Yan, B., 2023. Nanoplastic exposure at environmental concentrations disrupts hepatic lipid metabolism through oxidative stress induction and endoplasmic reticulum homeostasis perturbation. Environ. Sci. Technol. 57, 14127–14137.
Wang, J., Yu, P., Xie, X., Wu, L., Zhou, M., Huan, F., Jiang, L., Gao, R., 2021a. Bisphenol F induces nonalcoholic fatty liver disease-like changes: involvement of lysosome disorder in lipid droplet deposition. Environ. Pollut. 271, 116304.
WHO, 2022. Dietary and inhalation exposure to nano- and microplastic particles and potential implications for human health. https://www.who.int/publications/i/item/9789240054608.
Wright, S.L., Levermore, J.M., Kelly, F.J., 2019. Raman spectral imaging for the detection of inhalable microplastics in ambient particulate matter samples. Environ. Sci. Technol. 53, 8947–8956.
Yamamoto, H., Zhang, S., Mizushima, N., 2023. Autophagy genes in biology and disease. Nat. Rev. Genet. 24, 382–400.
Yanes, R.E., Tarn, D., Hwang, A.A., Ferris, D.P., Sherman, S.P., Thomas, C.R., Lu, J., Pyle, A.D., Zink, J.I., Tamanoi, F., 2013. Involvement of lysosomal exocytosis in the excretion of mesoporous silica nanoparticles and enhancement of the drug delivery effect by exocytosis inhibition. Small 9, 697–704.
Yang, S., Zhang, A., Li, T., Gao, R., Peng, C., Liu, L., Cheng, Q., Mei, M., Song, Y., Xiang, X., Wu, C., Xiao, X., Li, Q., 2017. Dysregulated autophagy in hepatocytes promotes bisphenol A-induced hepatic lipid accumulation in male mice. Endocrinology 158, 2799–2812.
Yao, M., Mu, L., Gao, Z., Hu, X., 2023. Persistence of algal toxicity induced by polystyrene nanoplastics at environmentally relevant concentrations. Sci. Total Environ. 876, 162853.
Yin, K., Wang, D., Zhao, H., Wang, Y., Zhang, Y., Liu, Y., Li, B., Xing, M., 2022. Polystyrene microplastics up-regulates liver glutamine and glutamate synthesis and promotes autophagy-dependent ferroptosis and apoptosis in the cerebellum through the liver-brain axis. Environ. Pollut. 307, 119449.
Yin, K., Wang, D., Zhang, Y., Lu, H., Hou, L., Guo, T., Zhao, H., Xing, M., 2023. Polystyrene microplastics promote liver inflammation by inducing the formation of macrophages extracellular traps. J. Hazard. Mater. 452, 131236.
Yu, Q., Wang, Y., Mei, R., Yin, Y., You, J., Chen, L., 2019. Polystyrene encapsulated SERS tags as promising standard tools: simple and universal in synthesis; highly sensitive and ultrastable for bioimaging. Anal. Chem. 91, 5270–5277.
Zhang, Y., Li, K., Kong, A., Zhou, Y., Chen, D., Gu, J., Shi, H., 2021b. Dysregulation of autophagy acts as a pathogenic mechanism of non-alcoholic fatty liver disease (NAFLD) induced by common environmental pollutants. Ecotoxicol. Environ. Saf. 217, 112256.
Zhang, J., Peng, M., Lian, E., Xia, L., Asimakopoulos, A.G., Luo, S., Wang, L., 2023. I dentification of poly(ethylene terephthalate) nanoplastics in commercially bottled drinking water using surface-enhanced raman spectroscopy. Environ. Sci. Technol. 57, 8365–8372.
Zhang, X., Wen, K., Ding, D., Liu, J., Lei, Z., Chen, X., Ye, G., Zhang, J., Shen, H., Yan, C., Dong, S., Huang, Q., Lin, Y., 2021a. Size-dependent adverse effects of microplastics on intestinal microbiota and metabolic homeostasis in the marine medaka (oryzias melastigma). Environ. Int. 151, 106452.
Zhao, Y., Mao, A., Zhang, R., Guan, S., Lu, J., 2022. SIRT1/mTOR pathway-mediated autophagy dysregulation promotes pb-induced hepatic lipid accumulation in HepG2 cells. Environ. Toxicol. 37, 549–563.
Zhong, G., Rao, G., Tang, L., Wu, S., Tang, Z., Huang, R., Ruan, Z., Hu, L., 2022. Combined effect of arsenic and polystyrene-nanoplastics at environmentally relevant concentrations in mice liver: activation of apoptosis, pyroptosis and excessive autophagy. Chemosphere 300, 134566.
Zhou, L., Yu, Z., Xia, Y., Cheng, S., Gao, J., Sun, W., Jiang, X., Zhang, J., Mao, L., Qin, X., Zou, Z., Qiu, J., Chen, C., 2022. Repression of autophagy leads to acrosome biogenesis disruption caused by a sub-chronic oral administration of polystyrene nanoparticles. Environ. Int. 163, 107220.